Free Radical Biology and Medicine 99 (2016) 179–188

Contents lists available at ScienceDirect

Free Radical Biology and Medicine

journal homepage: www.elsevier.com/locate/freeradbiomed

Original article

Increased obesity resistance and insulin sensitivity in mice lacking the isocitrate dehydrogenase 2 gene

Su Jeong Lee [a], Sung Hwan Kim [a], Kwon Moo Park [b], Jin Hyup Lee [c,d,**], Jeen-Woo Park [a,*]

[a] School of Life Sciences and Biotechnology, BK21 Plus KNU Creative BioResearch Group, College of Natural Sciences, Kyungpook National University, Taegu, Republic of Korea
[b] Department of Anatomy, School of Medicine, Kyungpook National University, Taegu, Republic of Korea
[c] Department of Food and Biotechnology, Korea University, Sejong, Republic of Korea
[d] Institutes of Natural Sciences, Korea University, Sejong, Republic of Korea

ARTICLE INFO

Article history:
Received 23 February 2016
Received in revised form
6 August 2016
Accepted 8 August 2016
Available online 9 August 2016

Keywords:
Reactive oxygen species
Isocitrate dehydrogenase 2
Obesity

ABSTRACT

Reactive oxygen species (ROS) are a byproduct of normal metabolism and play important roles in cell signaling and homeostasis. Mitochondria, the main organelles involved in intracellular ROS production, play central roles in modulating redox-dependent cellular processes such as metabolism and apoptosis. We recently reported an important role for mitochondrial $NADP^+$-dependent isocitrate dehydrogenase (IDH2) in cellular redox regulation. Here, we show that mice with targeted disruption of *IDH2* exhibit resistance to obesity, with lower body weight and reduced visceral fat, and increased insulin sensitivity accompanied by enhanced energy expenditure relative to controls. This function of IDH2 is linked to its capacity to suppress lipogenesis in visceral adipose tissue, partly via transcriptional repression of SREBP1, and to increase thermogenesis in adipocytes by transcriptional activation of UCP1 via activation of the p38 signaling axis. Our results highlight the importance of redox balance in the regulation of metabolism and demonstrate that IDH2 plays a major role in modulating both insulin sensitivity and fuel metabolism, thereby establishing this protein as a potential therapeutic target in the treatment of type 2 diabetes and obesity.

1. Introduction

Obesity is an increasingly prevalent medical and social problem with potentially devastating consequences as it clusters with type 2 diabetes, hypertension, atherosclerosis, and hyperlipidemia in metabolic syndrome or syndrome X [1,2]. Obesity is characterized by enlargement of visceral white adipose tissue (WAT) mass. Visceral fat enlargement encompasses an increase in both adipocyte cell size and cell number [3]. However, it is predominantly the increase in visceral adipocyte cell size, termed adipocyte hypertrophy, which is strongly influenced by lipid metabolism and linked to a greater susceptibility of developing obesity-related pathologies [4].

Obesity is associated with increased systemic oxidative stress, which may result from a combination of adipokine imbalance, comorbidities, and reduced antioxidant defenses [5]. In cross-sectional studies, obese subjects have exhibited higher levels of oxidative stress biomarkers compared with their leaner counterparts [6]. There are multiple sources of oxidative stress in relation to obesity. Some of these are inherently related to increased adiposity and fat distribution, whereas others are the result of comorbidities or behavioral lifestyle factors associated with being obese. Increased adipose tissue and, in particular, visceral adiposity with adipocyte hypertrophy are significantly related to systemic levels of oxidative stress [7]. In addition, recent studies have implicated systemic oxidative stress as a major contributing factor in obesity-related metabolic complications [6], and shown that oxidative stress in adipose tissue results in inflammation, adipokine dysregulation, and insulin resistance [8]. Since adipose tissue plays a crucial role in regulating whole-body obesity and insulin sensitivity [9], the balanced regulation of pro- and antioxidative mechanisms in adipocytes is important for the metabolic homeostasis.

Mitochondria are the main organelles involved in the production of reactive oxygen species (ROS). Additionally, these are the main targets of ROS-induced damage, as observed in various pathological states, including obesity [10,11]. The production of NADPH, which is required for the regeneration of glutathione in the mitochondria, is critical for the scavenging of mitochondrial ROS by glutathione reductase and peroxidase systems [12,13]. In

* Corresponding author.
** Corresponding author at: Department of Food and Biotechnology, Korea University, Sejong, Republic of Korea.
E-mail addresses: jinhyuplee@korea.ac.kr (J.H. Lee), parkjw@knu.ac.kr (J.-W. Park).

http://dx.doi.org/10.1016/j.freeradbiomed.2016.08.011
0891-5849/

addition, mitochondria relay information via several known retrograde signaling molecules such as ROS, Ca^{2+}, and cytochrome *c* [14]. Numerous studies suggest that mitochondrial ROS have evolved as key mediators of communication between the mitochondria and the cell for the regulation of homeostasis and maintenance of normal cellular function [15].

Mitochondrial $NADP^+$-dependent isocitrate dehydrogenase (IDH2), an NADPH-generating enzyme, is a major antioxidant and redox regulators that prevents oxidative stress by catalyzing the production of NADPH in mitochondria [16]. IDH2 is an evolutionarily conserved protein that catalyzes the oxidative decarboxylation of isocitrate into α-ketoglutarate and the reduction of $NADP^+$ to NADPH. IDH2 acts in the forward Krebs cycle as a $NADP^+$-consuming enzyme, generating NADPH for the maintenance of the reduced glutathione and peroxiredoxin systems, and for self-maintenance via the reactivation of cysteine-inactivated IDH2 by glutaredoxin 2 [17].

Mitochondria are the major source of intracellular ROS, and "mitochondrial fitness" plays a crucial role in the maintenance of adipocyte function [18]. As IDH2 is a major mitochondrial redox regulator, our study focuses on the role of endogenous IDH2, linking mitochondrial redox status and regulation of adipocyte function. We found that *IDH2*-deficient mice, which are resistant to diet-induced obesity, exhibit several metabolic changes related to glucose tolerance, insulin sensitivity, and hepatic steatosis. We propose that the negative effects of IDH2 on the SREBP1 metabolic regulatory system contribute to the suppression of genes involved in lipogenesis associated with visceral adipocyte hypertrophy. In addition, IDH2 disruption promotes increased energy expenditure via thermogenesis by regulating UCP1 expression through the induction of ROS accumulation in adipocytes. This metabolic phenotype is profoundly different from the metabolic syndrome observed in mice with disruption of general antioxidant enzymes, suggesting that IDH2 plays a major role in modulating both obesity and insulin sensitivity. Our findings therefore indicate that IDH2 may be a valuable therapeutic target in counteracting obesity and type 2 diabetes.

2. Materials and methods

2.1. Animal care and experimental protocol

The animals used in this study were *idh2*$^{-/-}$ germ-line knockout (*IDH2*$^{-/-}$) mice and their littermate WT control, and both mice are C57BL/6 J background [19]. The animals were housed in climate-controlled, specific pathogen-free barrier facilities under a 12-h light-dark cycle, and chow and water were provided *ad libitum*. The Institutional Animal Care and Use Committee at the Kyungpook National University approved the experimental protocols for this study. Mice were fed a normal chow diet (12% fat calories, Purina Laboratory Rodent Diets 38057) or a high-fat diet (60% fat calories, Research Diets D12492). The high-fat diet study with 6-month-old *IDH2*$^{-/-}$ mice and controls was followed for a period of 4 weeks. Body weights were measured daily during the experimental protocol. At the end of the experimental period, one mouse from each group was anesthetized, and the degree and distribution of adiposity was examined by computed tomography (CT) imaging. All other mice were euthanized, and dissected tissue specimens were immediately stored at −80 °C until analysis.

2.2. Physiological measurements

For measurement of food consumption, 10-month-old *IDH2*$^{-/-}$ mice and controls were housed individually. Food consumption and body weight was measured for 7 d consecutively. The surface temperature of the mice was imaged at 24 °C using a high-resolution infrared camera (Ti45-60HZ Thermal Imager, Fluke Corporation) and analyzed with a software package (SmartView 3.10 Software). Rectal temperature was monitored using an electronic thermistor (Model BAT-12) equipped with a rectal probe (RET-3, Physitemp).

2.3. Blood chemistry and metabolite analyses

For the intraperitoneal glucose tolerance test (IGTT), 10-month-old *IDH2*$^{-/-}$ mice and controls were deprived of food for 16 h and administered 0.75 mg glucose per g body weight intraperitoneally. For the intraperitoneal insulin tolerance test (IITT), 10-month-old *IDH2*$^{-/-}$ mice and controls were administered 0.75 U human insulin per kg of body weight by subcutaneous injection. Blood was withdrawn from the supraorbital vein at the indicated times. Blood glucose was measured by glucose oxidase method (Roche). Serum FFA, triglyceride, and total cholesterol levels were determined by the nonesterified fatty acid C-test, triglyceride L-type, and cholesterol L-type (Wako), respectively. LDL and HDL cholesterol levels were determined with HDL and LDL/VLDL assay Kit (Sigma Aldrich). Plasma insulin was measured by ELISA-based insulin immunoassay kit (Mercodia), according to the manufacturer's instructions. Liver tissues were excised, weighed, and homogenized. A 500 μl volume of homogenates was added to 3 mL of methanol/chloroform at a 1:2 (vol/vol) ratio. The mixture was shaken for 10 min and then centrifuged. The organic layer was removed and saved, the aqueous layer was re-extracted with 3 mL of methanol/chloroform, and a small aliquot of the combined organic extracts was evaporated. FFA and triglyceride concentration of this aliquot was determined as described earlier.

2.4. Histological analysis

Tissues were harvested and fixed in 4% (w/v) paraformaldehyde in PBS and embedded in paraffin. Then, 5-μm-thick tissue sections were deparaffinized, rehydrated, and used for H&E staining, immunohistochemistry, and immunofluorescence. For antigen retrieval, the slides were submerged in 10 mM sodium citrate (pH 6.0) and heated to 90 °C for 20 min. Tissue lipid content was assessed by Oil Red O or Nile red staining of paraffin-embedded tissue sections. Immunohistochemistry was performed using a VECTASTAIN ABC Kit (PK-4001, Vector Laboratories, Burlingame, CA, USA), according to the manufacturer's instructions, using antibody against UCP1 and PGC-1α (Abcam), SREBP1 (Santa Cruz Biotechnology), ACC, FAS, p-ATF-2, and p-p38 (Cell Signaling Technology), GSSG (ViroGen), and NADPH (Biorbyt). Antibodies used for immunofluorescence staining were anti-Opa1 (BD Bioscience), anti-Mfn1, and Fis1 (Sigma Aldrich). Images were acquired with a light microscope (Nikon Eclipse 80i) or a confocal microscope (Nikon E600). Staining intensities were analyzed using color deconvolution feature of ImageQuant 5.2 software (Molecular Dynamics).

2.5. CT scan analysis

The adiposity of mice was examined radiographically using the small animal Inveon system (Siemens Medical Solutions, USA). Briefly, the micro CT scanner was set to 80 kVp for the X-ray tube and 500 μA for the X-ray source, with an exposure time of 250 ms. The detector and X-ray source were rotated 360° with 180 rotation steps, the number of calibration exposures was 30, and the FOV was set as 56.89 × 56.89 mm. CT reconstruction was used to standardize the cone-beam setup with one of the values from the downsampling factors. The number of voxels for the bone scan

was $512 \times 512 \times 512$. The images were reconstructed in a short time using the modified Feldkamp process (Cobra EXXIM software, EXXIM Computing Corp). CT scanning was performed at 2-mm intervals, from the diaphragm to the bottom of the abdominal cavity.

2.6. Immunoblot analysis

Antibodies were from the following sources: UCP1, PGC-1α, and Prx-SO_3 (Abcam), SREBP1 and Actin (Santa Cruz Biotechnology), ACC, FAS, p-ATF-2, ATF-2, p-p38, p38, and p53 (Cell Signaling Technology), Opa1 (BD Bioscience), and Fis1 (Sigma Aldrich). Conventional immunoblotting procedures were used to detect the target proteins, as follows: Tissues were homogenized and lysed in TEGN buffer (10 mM Tris, pH 8, 1 mM EDTA, 10% glycerol, 0.5% Nonidet P-40, 400 mM NaCl, 1 mM DTT, 0.5 mM phenylmethylsulfonylfluoride and protease inhibitor mixture containing 1 M benzamidine, 3 mg/mL leupeptin, 100 mg/mL bacitracin, and 1 mg/mL α2 macroglobulin) and incubated on ice for 15 min. Lysates were then cleared by centrifugation at $20{,}000 \times g$ for 10 min. Total protein concentration was determined via the Bio-Rad protein assay. Equal amounts of protein were separated on 10% SDS/PAGE and the proteins were transferred to nitrocellulose membranes (Schleicher and Schuell). The membranes were blocked for 1 h in PBS solution containing 5% nonfat milk powder and 0.1% Tween-20 and then probed with primary antibody overnight in 1% milk and 0.1% Tween-20 in PBS. Finally, after three 5-min washes in 0.1% PBS/Tween-20, proteins were visualized by enhanced chemiluminescence (Amersham Biosciences). Band intensities were quantified with ImageQuant 5.2 software (Molecular Dynamics).

2.7. Reverse transcription-polymerase chain reaction (RT-PCR)

RNA was extracted using an RNeasy Mini Kit (Qiagen) and quantified by UV–vis spectrophotometry. The cDNAs were generated by reverse transcription with random hexamers using the ImProm-II Reverse Transcription System (Promega). Then, RT-PCR was performed with the primers listed in Supplementary Table 1, using the GeneAmp 2400 PCR System (Perkin-Elmer Cetus) according to the manufacturer's protocol. PCR products were separated on 2% agarose gels and bands were visualized with ethidium bromide staining.

2.8. Measurement of redox status and cellular ROS

Intracellular peroxide concentrations were determined using a ferric acid-sensitive dye, xylenol orange, as previously described [20]. The concentration of total glutathione was determined by the rate of formation of 5-thio-2-nitrobenzoic acid at 412 nm ($\varepsilon = 1.36 \times 10^4\ M\ M^{-1}\ cm^{-1}$) according to the method described by Akerboom and Sies [21]. Oxidized glutathione (GSSG) was measured by the 5,5′-dithiobis(2-nitrobenzoic acid)-GSSG reductase recycling assay after treating GSH with 2-vinylpryidine [22]. NADPH was measured using the enzymatic cycling method as described by Zerez et al. [23] and expressed as the ratio of NADPH to the total NADP pool. Intracellular ATP levels were determined by using luciferin-luciferase, as previously described [24]. Light emission was quantitated in a Turner Designs TD 20/20 luminometer (Stratec Biomedical Systems). In order to examine the levels of mitochondrial ROS, DHR 123 (Dihydrorhodamine 123; 2 mg/kg body weight) was administered intraperitoneally and then tissues were homogenized and lysed in TEGN buffer. Fluorescence intensity was analyzed using a Shimadzu UV1650 spectrophotometer using excitation and emission wavelengths of 500 and 536 nm, respectively.

2.9. Statistical analysis

Analyses were performed using a two-tailed *t*-test. Results are shown as means ± SD.

3. Results

3.1. Disruption of IDH2 in vivo

In order to investigate the physiological role of IDH2, we generated mice with mutation in *IDH2*, leading to IDH2 deficiency (Supplementary Fig. 1). Notably, $IDH2^{-/-}$ mice exhibited an obese-resistant phenotype compared with wild-type mice, even when a normal diet is administered, suggesting that IDH2 plays a crucial role in regulating adiposity in adulthood (Fig. 1A). We therefore focused on elucidating the role of IDH2 in the pathogenesis of obesity and associated disorders.

3.2. Resistance to obesity in $IDH2^{-/-}$ mice

There was no difference in body weight at birth between genotypes; however, at 24 weeks, the body weight of $IDH2^{-/-}$ mice was lower than that of wild-type mice. This difference in body weight was found to persist throughout their lives, when fed on a normal diet (Fig. 1B). There were no phenotypic differences between male and female mice. 10-month-old $IDH2^{-/-}$ mice showed a marked reduction in body weight compared with wild-type mice (Fig. 1C). Furthermore, macroscopic and computed tomographic (CT) analyses taken 10 months after birth showed that visceral fat depots were significantly lower in $IDH2^{-/-}$ mice compared with in wild-type mice (Fig. 1D). However, there was no significant difference in the weights of other organs such as lung, kidney, and spleen, referring to body weight normalized (Supplementary Fig. 2A). In contrast, visceral white adipose tissue (WAT) per body weight in $IDH2^{-/-}$ mice was markedly lower than that in wild-type mice (Fig. 1E). Consistent with fat mass reduction, sections of WAT from $IDH2^{-/-}$ mice showed decreased adipocyte size relative to wild-type mice (Fig. 1F and G). Furthermore, a smaller amount of lipid accumulation in the adipose tissue was observed in $IDH2^{-/-}$ mice than in wild-type mice, indicating that a reduction in total fat mass results from decreased triglyceride accumulation (Supplementary Fig. 2B). In order to further investigate whether $IDH2^{-/-}$ mice show resistance to diet-induced obesity, we challenged the two genotypes with a high-fat diet containing 60% (wt/wt) fat for 28 days to stimulate weight gain. $IDH2^{-/-}$ mice fed this diet showed significant differences associated with reduction in body weight compared to wild-type mice (Fig. 1H and I). At the end of the feeding period, the net weight gains were 3.12 ± 1.67 g and 11.79 ± 2.06 g, respectively, for $IDH2^{-/-}$ mice and wild-type mice (Fig. 1J). However, there was no significant difference in apparent food consumption between the two genotypes (Supplementary Fig. 3A). As expected, administering a high-fat diet caused massive lipid accumulation in visceral fat depots in the controls, whereas such changes were rarely seen in $IDH2^{-/-}$ mice (Fig. 1K and L; Supplementary Fig. 3B). Notably, the adipocyte size of visceral WAT in $IDH2^{-/-}$ mice was markedly smaller than that in wild-type mice (Fig. 1M and N).

3.3. Metabolic alterations in $IDH2^{-/-}$ Mice

There was no difference in in vitro adipocyte differentiation of embryonic fibroblasts between $IDH2^{-/-}$ mice and wild-type mice (data not shown). In order to investigate alternative causes of decreased adiposity in $IDH2^{-/-}$ mice, we compared lipid metabolism, body temperature, and food intake in $IDH2^{-/-}$ mice and

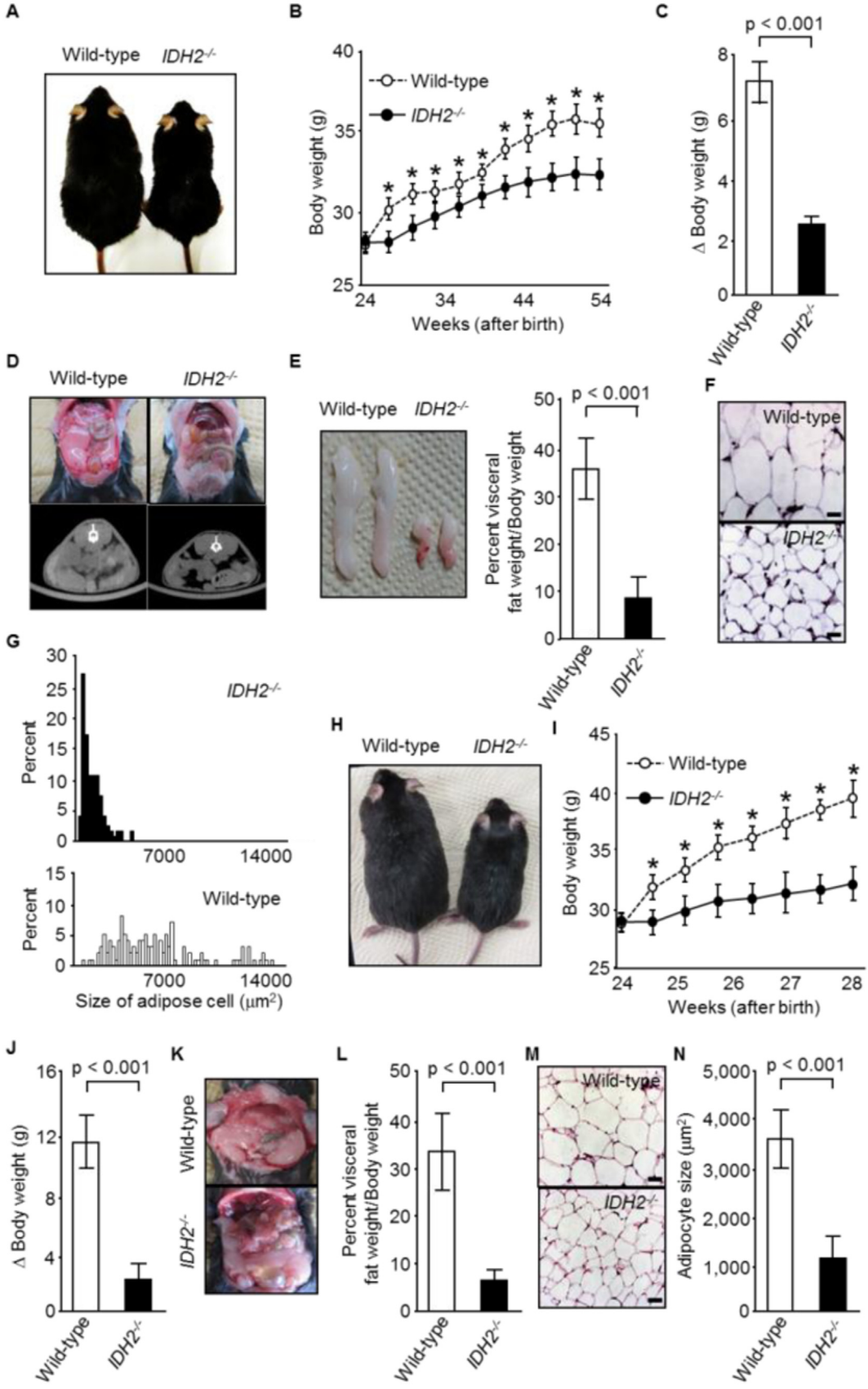

Fig. 1. Resistance to obesity in *IDH2*$^{-/-}$ mice. (A) Gross appearance of 10-month-old wild-type and *IDH2*$^{-/-}$ mice on a normal diet. (B) Body weight of wild-type and *IDH2*$^{-/-}$ mice on a normal diet ($n=10$). (C) Change in body weight of wild-type and *IDH2*$^{-/-}$ mice fed a normal diet for 4 months, starting at 6 months of age ($n=10$). (D) Abdominal cavity and representative cross-sectional CT images of 10-month-old wild-type and *IDH2*$^{-/-}$ mice fed a normal diet. (E) Gross image of visceral fat and visceral WAT weight/body weight of 10-month-old wild-type and *IDH2*$^{-/-}$ mice on a normal diet ($n=7$). (F) Hematoxylin and eosin (H&E)-stained sections and (*G*) distribution of adipocyte size in visceral WAT from 10-month-old wild-type and *IDH2*$^{-/-}$ mice on a normal diet ($n=3$). The diameters of visceral white adipocytes were determined by ImageQuant. More than 500 adipocytes were examined for each group. (H) Photograph of 6-month-old wild-type and *IDH2*$^{-/-}$ mice showing body size differences after 4 weeks of a high-fat diet. (I) Body weight of wild-type and IDH2$^{-/-}$ mice on a high-fat diet ($n=10$). (J) Change in body weight of 6-month-old wild-type and *IDH2*$^{-/-}$ mice after 4-weeks of high-fat feeding ($n=10$). (K) Macroscopic level, (L) comparison of visceral fat weight/body weight ($n=7$), (M) histological analysis, and (*N*) Average adipocyte sizes in visceral WAT from 6-month-old wild-type and *IDH2*$^{-/-}$ mice after 4 weeks of a high-fat diet ($n=3$). Data are presented as means ± SD. Bars in histological sections indicate 50 μm. *$P<0.01$ between the two genotypes indicated. The figure shows representative data for three independent experiments. Male mice were used for all experiments.

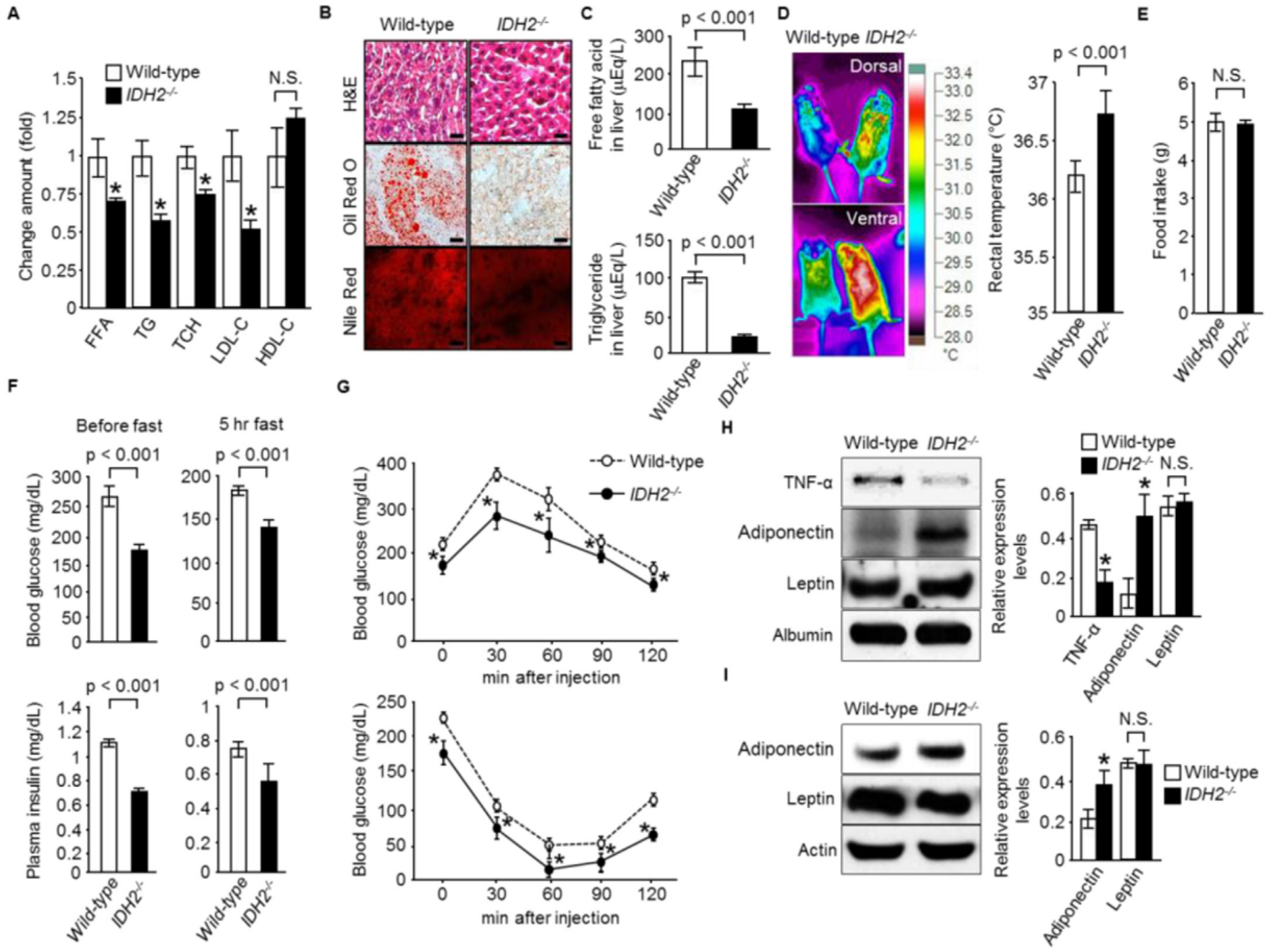

Fig. 2. Metabolic effects of *IDH2* deficiency on a normal diet. (A) Plasma concentrations of free fatty acid (FFA), triglyceride (TG), total cholesterol (TCH), LDL cholesterol (LDL-C), HDL cholesterol (HDL-C) in wild-type and $IDH2^{-/-}$ mice. Values are presented as the fold change over the levels observed in wild-type mice. (B) Representative H&E-stained and lipid-stained sections from livers of wild-type and $IDH2^{-/-}$ mice. (C) Hepatic concentrations of FFA and triglyceride in wild-type and $IDH2^{-/-}$ mice. (D) Representative infrared thermal images of temperature of the skin and quantification of rectal temperature in wild-type and $IDH2^{-/-}$ mice. (E) Average food intake of wild-type and $IDH2^{-/-}$ mice. (F) Plasma glucose levels and insulin concentration in wild-type and $IDH2^{-/-}$ mice before and after 5-h fast. (G) Glucose and insulin tolerance tests in wild-type and $IDH2^{-/-}$ mice. (H) Immunoblots comparing the levels of adiponectin, TNF-α, and leptin in the serum of wild-type and $IDH2^{-/-}$ mice. Albumin served as a loading control. Quantification of adiponectin, TNF-α, and leptin levels normalized to albumin is shown. (I) Immunoblot analysis of adiponectin and leptin expression in visceral WAT of wild-type and $IDH2^{-/-}$ mice. Actin was used as a loading control. The protein levels were normalized to the actin level. Each value represents the mean ± SD from five to six independent experiments. $^{*}P < 0.01$, between the two genotypes indicated. N.S. indicates no significant difference compared with wild-type mice. The figure shows representative data for five independent experiments. Bars in histological sections indicate 50 μm. 10-month-old male mice were used for all experiments.

wild type mice. Significant reductions were observed in the levels of plasma total cholesterol, free fatty acid (FFA), LDL cholesterol, and triglycerides in $IDH2^{-/-}$ mice; however there was no significant difference in serum HDL cholesterol concentration between the two genotypes (Fig. 2A). As the plasma lipid metabolites observed above are closely associated with hepatic steatosis in obesity [25], we also studied the effect of the metabolic alterations on the development of hepatic steatosis. Remarkably, histological examination of liver tissue from $IDH2^{-/-}$ mice revealed a reduction in lipid droplets and decreased accumulation of triglyceride compared with wild-type mice (Fig. 2B), indicating amelioration of hepatic steatosis in $IDH2^{-/-}$ mice. Consistent with the reduced lipid deposition in the liver, hepatic triglyceride levels and FFA contents were markedly decreased in $IDH2^{-/-}$ mice (Fig. 2C). $IDH2^{-/-}$ mice also showed significant increases in ambient and rectal core body temperature compared with wild-type mice (Fig. 2D), suggesting enhanced energy expenditure in $IDH2^{-/-}$ mice. The daily food intake in $IDH2^{-/-}$ mice, however, was similar to that in wild-type mice when individually housed and fed a normal diet (Fig. 2E).

3.4. Insulin sensitivity in $IDH2^{-/-}$ mice

Obesity is a major risk factor for insulin resistance as well as type 2 diabetes. Adipose tissue, in particular, has a substantial effect on systemic glucose homeostasis via secretion of adipocytokines [26]. In order to investigate this further, we performed intraperitoneal glucose and insulin tolerance tests (IGTT and IITT, respectively). As expected, the circulating glucose and insulin levels were observed to be significantly lower in $IDH2^{-/-}$ mice than in wild-type mice (Fig. 2F). IGTT and IITT showed that $IDH2^{-/-}$ mice exhibit improved glucose tolerance and increased insulin sensitivity (Fig. 2G). Recent studies have demonstrated that tumor necrosis factor (TNF)-α [27] secreted from adipose tissue acts as a mediator of insulin resistance, and that adiponectin [28] and leptin [29] mediate insulin sensitivity. $IDH2^{-/-}$ mice showed increased serum adiponectin levels and decreased serum TNF-α level, whereas no significant differences were observed in leptin

concentration in serum between genotypes (Fig. 2H). Additionally, adiponectin levels in the adipocytes of *IDH2*$^{-/-}$ mice were markedly higher than those in the adipocytes of wild-type mice, whereas the leptin levels in the adipocytes did not significantly differ between the genotypes (Fig. 2I), suggesting that adipose tissues in *IDH2*$^{-/-}$ mice secrete adiponectin at high levels, and the increased glucose tolerance and insulin sensitivity observed in *IDH2*$^{-/-}$ mice directly result from the increased serum adiponectin. Taken together, these results clearly show that *IDH2*$^{-/-}$ mice exhibit obesity resistance-related insulin sensitivity and glucose metabolism.

3.5. Molecular alterations in *IDH2*$^{-/-}$ mice

The physiological data presented above indicate that the inactivation of IDH2 in vivo leads to resistance to obesity, which is associated with resistance to adipocyte hypertrophy and increased energy expenditure. It is well established that, together with excess energy intake, an increase in lipogenesis in adipose tissue causes adipocyte hypertrophy and thermogenesis, i.e., heat production in response to food intake and changes in environmental temperature, is an important defense against obesity associated with increased energy expenditure [30]. In order to elucidate the molecular basis of these metabolic changes in *IDH2*$^{-/-}$ mice, we examined the expression of molecules with proposed roles in obesity that is associated with metabolic activity in adipocytes. Consistent with the reduced plasma lipid content in *IDH2*$^{-/-}$ mice, the expression of lipogenic genes such as sterol regulatory element binding protein 1 (SREBP1), fatty acid synthase (FAS), and acetyl-CoA carboxylase (ACC) was significantly lower in the adipocytes of *IDH2*$^{-/-}$ mice than in those of wild-type mice (Fig. 3A; Supplementary Fig. 4A). SREBP1, which is considered a key transcriptional regulator of triglyceride synthesis, controls the transcription and expression of lipogenic enzymes such as FAS, which catalyzes the first committed step in lipogenesis, and ACC, the rate-limiting enzyme in fatty acid synthesis [31]. RT-PCR analysis confirmed the downregulation of lipogenesis-related genes as well as *Scd1* and *Me1*, which are direct targets of SREBP1 involved in lipogenesis in the adipocytes of *IDH2*$^{-/-}$ mice (Fig. 3B). Recently, it was reported that the tumor suppressor p53 represses the promoter activity of the SREBP1 gene and its downstream gene, constituting a negative feedback loop against excess fat accumulation in adipocytes [32]. It was found that p53 is highly induced in the adipocytes of *IDH2*$^{-/-}$ mice compared with those of wild-type

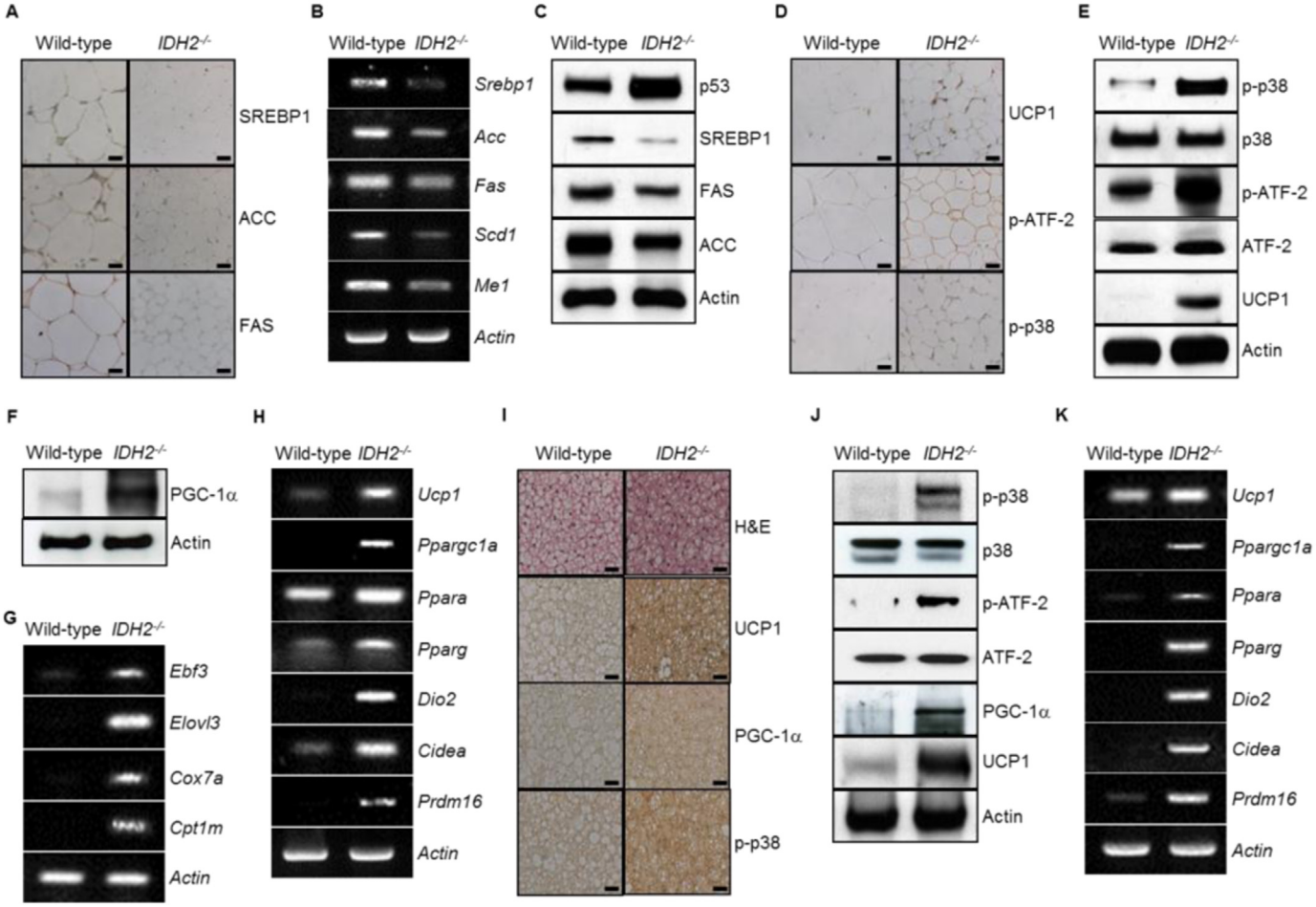

Fig. 3. Suppressed lipogenesis and increased thermogenesis in adipose tissues of *IDH2*$^{-/-}$ mice on a normal diet. (A) Immunohistochemical staining of proteins related to lipogenesis in visceral WAT of wild-type and *IDH2*$^{-/-}$ mice. (B) RT-PCR analysis of expression of genes associated with lipogenesis from visceral WAT of wild-type and *IDH2*$^{-/-}$ mice. *Actin* was used as an internal control for the experiment. (C) Immunoblot analysis of p53 levels and lipogenic protein expression in visceral WAT of wild-type and *IDH2*$^{-/-}$ mice. Actin was used as a loading control. (D) Immunohistochemical and (E) immunoblot analysis for protein expression of UCP1 and p38 MAPK activation from visceral WAT of wild-type and *IDH2*$^{-/-}$ mice. (F) Immunoblot analysis of PGC-1α expression in visceral WAT of wild-type and *IDH2*$^{-/-}$ mice. (G) RT-PCR analysis of mRNA levels of genes involved in brown fat-like changes in visceral WAT of wild-type and *IDH2*$^{-/-}$ mice. (H) RT-PCR analysis of thermogenic gene expression from visceral WAT of wild-type and *IDH2*$^{-/-}$ mice. (I) Representative images of H&E staining and immunohistochemical staining of proteins associated with thermogenesis in BAT of wild-type and *IDH2*$^{-/-}$ mice. (J) Immunoblot analysis of proteins related to p38-mediated UCP1 expression in BAT of wild-type and *IDH2*$^{-/-}$ mice. (K) RT-PCR analysis of genes involved in thermogenesis of BAT from wild-type and *IDH2*$^{-/-}$ mice. The figure shows representative data for three independent experiments. Bars in histological sections indicate 50 μm. 10-month-old male mice were used for all experiments.

mice, suggesting that p53 suppresses lipogenesis-related genes in the adipocytes of *IDH2*$^{-/-}$ mice by inhibiting SREBP1 expression (Fig. 3C; Supplementary Fig. 4B). It is well established that uncoupling protein 1 (UCP1) is a key contributor to browning of visceral WAT with thermogenesis. The brown fat-like cells in the adipose tissue have been associated with resistance to diet-induced obesity and improved glucose metabolism [33]. Several reports have shown that the activation of p38 mitogen-activated protein kinase (MAPK) in adipocytes is indispensable for the transcription of the UCP1 gene through phosphorylation of activating transcription factor 2 (ATF-2) [34]. UCP1 expression is significantly increased in visceral WAT of *IDH2*$^{-/-}$ mice and its expression is highly related to the increased activation of the p38-ATF-2 axis (Fig. 3D and E; Supplementary Fig. 4C). In addition, the activation of p38 has been shown to increase the expression of PGC-1α, a key coactivator of the thermogenic transcriptional program in browning of WAT (Fig. 3F; Supplementary Fig. 4A) [33]. To investigate if mitochondrial contents in the adipose tissue of *IDH2*$^{-/-}$ mice would be influenced by the activation of PGC-1α [35], mitochondrial contents were measured by immunohistochemistry for a mitochondrial marker protein, voltage-dependent anion channel (VDAC), and there was no significant change in the mitochondrial contents in both genotypes (Supplementary Fig. 5). These results indicate that the mitochondrial contents may not be influenced by the PGC-1α expressed in the tissues of *IDH2*–deficient mice. Gene expression analysis confirmed the induction of *Ppargc1a* (encoding PGC-1α, peroxisome proliferator-activated receptor γ coactivator 1α) as well as a number of its target genes associated with thermogenesis in WAT of *IDH2*$^{-/-}$ mice (Fig. 3G and H; Supplementary Fig. 4E), suggesting increased browning of WAT, and, therefore, thermogenesis in *IDH2*$^{-/-}$ mice. It is well-known that brown adipose tissue (BAT) is the primary site of energy expenditure by thermogenesis, which is mediated by UCP1 in mitochondria [36]. Interestingly, a markedly lower accumulation of lipid vesicles and higher expression of UCP1 was observed in BAT of *IDH2*$^{-/-}$ mice compared with those in wild-type mice (Fig. 3I; Supplementary Fig. 4F). Moreover, sections of BAT from *IDH2*$^{-/-}$ mice showed increased p38 phosphorylation levels (Fig. 3J; Supplementary Fig. 4G), which are significantly related to the increased expression of UCP1 via the p38-ATF-2 axis signaling pathway (Fig. 3J). In addition, phosphorylation and activation of p38 was found to stimulate the expression of PGC-1α in BAT (Fig. 3I and J). RT-PCR analysis showed significant increases in the expression of genes associated with thermogenesis in BAT of *IDH2*$^{-/-}$ mice (Fig. 3K). These findings suggest that the inactivation of IDH2 in vivo inhibits expression of lipogenesis-related genes and activates molecules involved in stimulating energy expenditure via thermogenesis in adipocytes, thereby, in part, leading to decreased adiposity.

3.6. Modulation of ROS production in *IDH2*$^{-/-}$ mice

Next, we attempted to elucidate the mechanisms by which IDH2 inactivation leads to elevation of the activity of these signaling axes. It is well established that coordination between mitochondrial and nuclear activities is vital for cellular homeostasis, and several signaling molecules and transcription factors, such as p38 MAPK and the tumor suppressor p53, are regulated by mitochondria-derived cellular ROS to carry out this interorganellar communication [37–39]. In particular, IDH2 is a primary NADPH producer in the mitochondria, which plays a critical role in cellular redox regulation by maintaining a NADPH-dependent GSH/GSSG ratio [16]. Therefore, this suggests that IDH2 modulates the cellular redox status responsible for the regulation of the signaling pathway. In order to examine the effect of IDH2 activity on redox status of mitochondria and subsequent cellular ROS production, we analyzed the mitochondrial redox (Fig. 4A), mitochondrial biogenesis (Fig. 4B), and intracellular ROS (Fig. 4C and D) in white adipocytes for the 2 genotypes. The data reveal that IDH2 inactivation leads to elevated levels of mitochondrial ROS and dynamic changes in mitochondrial morphology, leading to an increase in cellular ROS levels in the adipocytes. Furthermore, high levels of mitochondrial biogenesis (Fig. 4E) and increased cellular ROS levels (Fig. 4F and G), which are characteristic features of brown adipocytes essential for BAT-dependent thermogenesis, are also observed in BAT from *IDH2*$^{-/-}$ mice. Taken together, the data in Fig. 4 indicate that IDH2 inhibition, resulting in elevated cellular ROS production, gates the p38 MAPK-mediated thermogenic and the p53-mediated lipogenic axes in the adipose tissue. Fig. 4H summarizes the findings of this study as follows: the inhibition of IDH2 results in elevated intracellular ROS levels, which leads to the activation of UCP1 and inhibition of lipogenesis-related genes. This occurs via gating of the ROS-mediated p38-ATF-2 axis and p53-SREBP1 axis as a result of the modulation of cellular redox status. These data therefore indicate a critical role for ROS in lipid metabolism.

4. Discussion

Mitochondrial $NADP^+$-dependent isocitrate dehydrogenase, encoded by the *IDH2* gene, plays a major role in the regulation of redox balance and oxidative stress levels which are tightly associated with intermediary metabolism and energy production [40]. In order to establish the role of IDH2 in the metabolic phenotype in vivo, we generated *IDH2*-deficient mice using embryonic stem cells from C57BL mice and demonstrated that the inactivation of IDH2 in vivo has substantial metabolic benefits such as resistance to obesity and obesity-related metabolic disorders. *IDH2*-deficient mice are protected against diet-induced weight gain via the reduction of adipocyte hypertrophy, which results from the inhibition of the expression of genes associated with lipogenesis in adipose tissue. Furthermore, as a result of higher levels of UCP1 expression in their adipocytes, *IDH2*-deficient mice show increased energy expenditure through thermogenesis.

In the present study, we demonstrate a physiological role for mitochondrion-generated ROS in regulating metabolism in adiposity. We suggest that elevated mitochondrial ROS levels, resulting from the inhibition of IDH2, lead to higher UCP1 expression through p38 MAPK activation. This is consistent with the well-known relationship between ROS, p38 MAPK signaling, and UCP1 expression [34,41]. Recent studies have demonstrated that inhibition of ROS by chemical antioxidants was sufficient to inhibit both p38 MAPK activation and UCP1 expression, indicating that ROS is essential for inducible UCP1 expression and UCP1-mediated thermogenesis in adipocytes, and for homeostatic regulation of energy metabolism [42]. We then investigated the molecular mechanism underlying the reduction of adipocyte hypertrophy associated with decreased visceral fat mass. Interestingly, we found that inactivation of IDH2 suppresses the expression of lipogenesis-related genes via transcriptional repression of SREBP1, which is gated by ROS-mediated p53 activation. The tumor suppressor protein p53 is considered a redox active transcription factor that organizes and directs cellular responses against a variety of insults to genomic instability [39,43]. Recent studies have revealed that the cellular concentration and distribution of p53 are associated with distinct cellular functions. Additionally, it has been demonstrated that ROS act as both upstream signals that trigger p53 activation and as downstream factors that mediate the expression of key metabolic enzymes, orchestrating an intricate balance between mitochondrial respiration, glycolysis, and the pentose phosphate shunt [39]. p53 functions as a negative

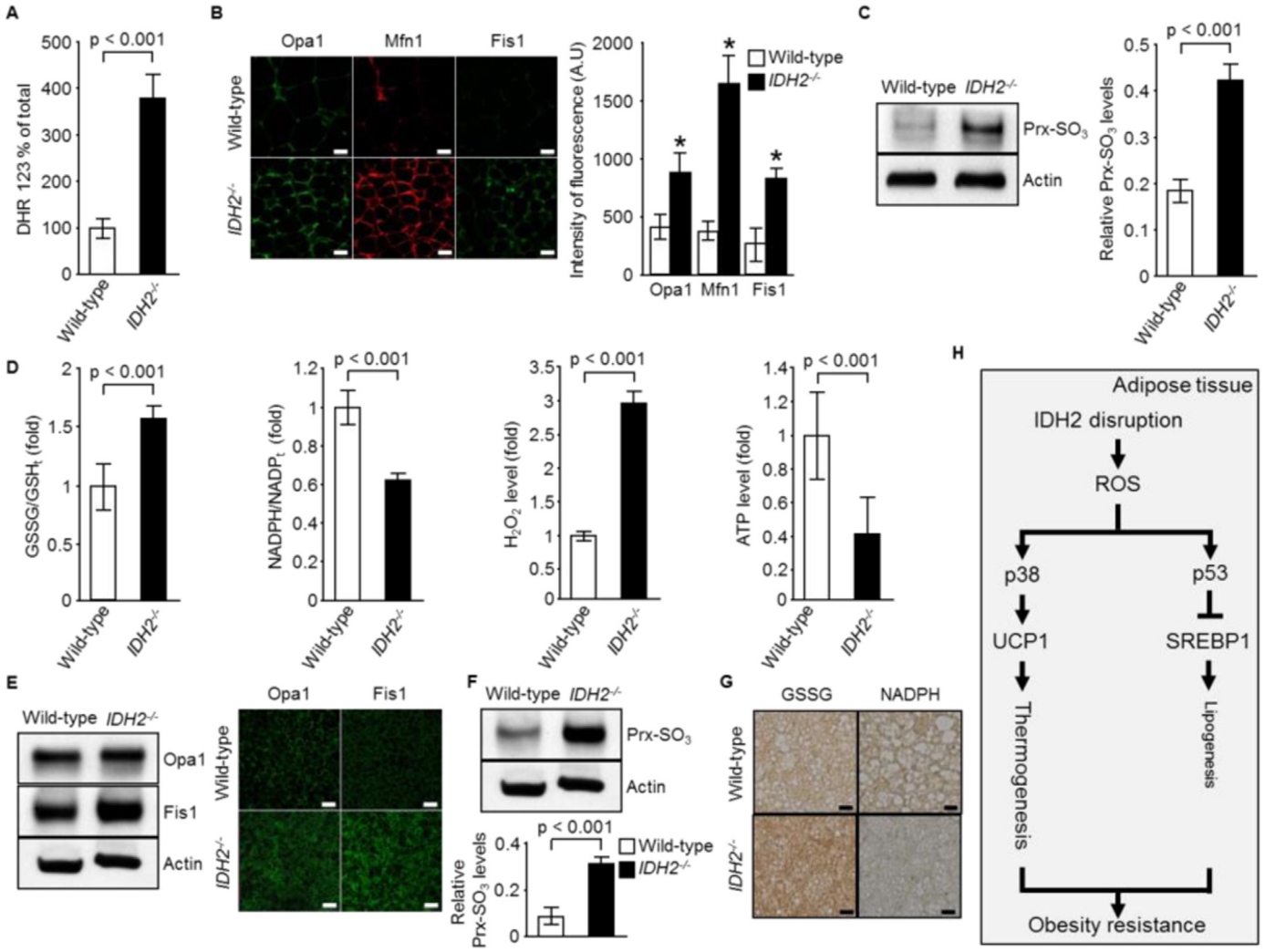

Fig. 4. The effect of *IDH2* deficiency on the modulation of redox status in adipose tissues. (A) Quantification of DHR 123 fluorescence level for evaluation of mitochondrial ROS generation in visceral WAT of wild-type and *IDH2*$^{-/-}$ mice. (B) Immunofluorescence staining of mitochondrial fusion markers Opa1/Mfn1 and a fission marker Fis1 in visceral WAT of wild-type and *IDH2*$^{-/-}$ mice. Histograms represent the quantification of fluorescence intensity. (C) Immunoblot analysis of oxidized peroxiredoxin (Prx-SO_3) level, a marker for intracellular ROS formation, in visceral WAT of wild-type and *IDH2*$^{-/-}$ mice. Actin was used as a loading control. The protein levels were normalized to the actin level. (D) Ratio of GSSG versus total GSH concentration, ratio of NADPH versus total NADP concentration, intracellular peroxide production, and ATP levels were measured in visceral WAT of wild-type and *IDH2*$^{-/-}$ mice. Values are presented as the fold change over the levels observed in wild-type mice. (E) Immunoblot and immunohistochemical analysis of mitochondrial fusion and fission markers related to mitochondrial biogenesis from BAT of wild-type and *IDH2*$^{-/-}$ mice. (F) Immunoblot analysis of Prx-SO_3 level in BAT of wild-type and *IDH2*$^{-/-}$ mice. Actin was used as a loading control. Quantifications of protein levels normalized to actin are shown. (G) Immunohistochemical staining of GSSG and NADPH for evaluation of intracellular redox status in BAT of wild-type and *IDH2*$^{-/-}$ mice. (H) Model for the regulation of UCP1-mediated thermogenesis and SREBP1-mediated lipogenesis through ROS-controlled p38 MAPK and p53 activity, respectively, resulting in IDH2 inactivation. Each value represents the mean ± SD from five to six independent experiments. *$P < 0.01$, between the two genotypes indicated. N.S. indicates no significant difference compared with wild-type mice. The figure shows representative data for five independent experiments. Bars in histological sections indicate 50 μm. 10-month-old male mice were used for all experiments.

regulator of lipid synthesis by activating fatty acid oxidation and inhibiting fatty acid synthesis [44]. In particular, activated p53 inhibits adipocyte differentiation and p53 knockout enhances lipid accumulation [45]. Of interest, p53 has been demonstrated to regulate key transcription factors responsible for the expression of genes involved in determining cellular lipogenic status e.g., SREBP1, which is a key transcription factor for genes involved in fatty acid synthesis [44]. p53 activation by ROS suppresses the expression of the SREBP1 in adipose tissue, contributing to the repression of FAS and ATP citrate lyase (ACLY) [32]. Disruption of p53 in *ob/ob* mice was found to partially restore SREBP1-mediated expression of lipogenic enzymes, constituting a negative feedback loop against excess fat accumulation in adipocytes [32]. Meanwhile, it is possible that IDH2 disruption is likely to induce various compensatory responses for counteracting the obesity-related metabolisms, which may not be directly related to ROS-mediated inhibition of SREBP1 and lipogenesis, and concomitant upregulation of UCP1 associated with thermogenesis. For example, it is plausible that *IDH2*-deficient mice appear to promote lipid catabolism more readily than that in wild-type mice due, in part, to compensatory increases in levels of component of fatty acid oxidation, and thus elevated rates of fatty acid oxidation, which is inferred by elevation of fatty acid metabolism-related genes as shown in Fig. 3F and H. Further detailed characterization and analyses are required to reveal the possibility in a future study.

Chronically elevated levels of cellular ROS have been attributed to diseases such as obesity and diabetes [8]. Several previous studies have suggested ROS as initiators of cellular damage. A plethora of recent studies, however, have proposed that, at physiological levels, ROS can also serve as signaling molecules to regulate normal physiological processes such as oxygen sensing [46]. Furthermore, over the last decade, our knowledge of ROS has

become more complex, as several reports have suggested that the type and the compartmentalization of ROS are likely to regulate distinct biological outcomes [47].

Antioxidants were once considered beneficial for treating age- and obesity-associated metabolic derangements such as chronic inflammation, fibrotic damage, and insulin resistance [48]. However, several animal and human clinical studies failed to show the benefits of antioxidants in treating age- or obesity-associated diseases [49] and instead revealed several harmful side effects [50,51]. It is plausible that antioxidant therapies may have interfered with certain ROS-dependent physiological processes important for metabolic homeostasis. The present study suggests that ROS-mediated inhibition of SREBP1 expression and concomitant promotion of UCP1 expression may override any beneficial effects of antioxidants.

In summary, we provide the first evidence that IDH2, as a central regulator of adipocyte lipid metabolism and energy expenditure, directly antagonizes obesity and obesity-related insulin resistance. Therefore, IDH2 is a potential target for the development of pharmacological interventions counteracting obesity and obesity-related metabolic diseases.

Acknowledgements

S.J.L., J.H.L, and J.P. designed research; S.J.L and K.M.P performed research; S.J.L, J.H.L, and J.P analyzed data; and J.H.L and J.P wrote the paper. The authors acknowledge the services of Division of Magnetic Resonance Research at the Ochang Center of Korea Basic Science Institute (KBSI). This work was supported by the National Research Foundation of Korea (NRF) grants funded by the Korea Government (MSIP) (NRF-2015R1A4A1042271) and granted by Korea University. No potential conflicts of interest relevant to this article were reported.

Appendix A. Supplementary material

Supplementary data associated with this article can be found in the online version at http://dx.doi.org/10.1016/j.freeradbiomed.2016.08.011.

References

[1] B.M. Spiegelman, J.S. Flier, Obesity and the regulation of energy balance, Cell 104 (4) (2001) 531–543.
[2] P.G. Kopelman, Obesity as a medical problem, Nature 404 (6778) (2000) 635–643.
[3] C.T. Montague, S. O'Rahilly, The perils of portliness: causes and consequences of visceral adiposity, Diabetes 49 (6) (2000) 883–888.
[4] S.L. Doyle, C.L. Donohoe, J. Lysaght, J.V. Reynolds, Visceral obesity, metabolic syndrome, insulin resistance and cancer, Proc. Nutr. Soc. 71 (1) (2012) 181–189.
[5] M. Sankhla, T.K. Sharma, K. Mathur, J.S. Rathor, V. Butolia, A.K. Gadhok, S. K. Vardey, M. Sinha, G.G. Kaushik, Relationship of oxidative stress with obesity and its role in obesity induced metabolic syndrome, Clin. Lab. 58 (5–6) (2012) 385–392.
[6] J.F. Keaney Jr., M.G. Larson, R.S. Vasan, P.W. Wilson, I. Lipinska, D. Corey, J. M. Massaro, P. Sutherland, J.A. Vita, E.J. Benjamin, S. Framingham, Obesity and systemic oxidative stress: clinical correlates of oxidative stress in the Framingham Study, Arterioscler. Thromb. Vasc. Biol. 23 (3) (2003) 434–439.
[7] K. Fujita, H. Nishizawa, T. Funahashi, I. Shimomura, M. Shimabukuro, Systemic oxidative stress is associated with visceral fat accumulation and the metabolic syndrome, Circ. J. 70 (11) (2006) 1437–1442.
[8] S. Furukawa, T. Fujita, M. Shimabukuro, M. Iwaki, Y. Yamada, Y. Nakajima, O. Nakayama, M. Makishima, M. Matsuda, I. Shimomura, Increased oxidative stress in obesity and its impact on metabolic syndrome, J. Clin. Investig. 114 (12) (2004) 1752–1761.
[9] H. Bays, L. Mandarino, R.A. DeFronzo, Role of the adipocyte, free fatty acids, and ectopic fat in pathogenesis of type 2 diabetes mellitus: peroxisomal proliferator-activated receptor agonists provide a rational therapeutic approach, J. Clin. Endocrinol. Metab. 89 (2) (2004) 463–478.
[10] R.S. Balaban, S. Nemoto, T. Finkel, Mitochondria, oxidants, and aging, Cell 120 (4) (2005) 483–495.
[11] D.C. Chan, Fusion and fission: interlinked processes critical for mitochondrial health, Annu. Rev. Genet. 46 (2012) 265–287.
[12] O.W. Griffith, A. Meister, Origin and turnover of mitochondrial glutathione, Proc. Natl. Acad. Sci. USA 82 (14) (1985) 4668–4672.
[13] J. Martensson, J.C. Lai, A. Meister, High-affinity transport of glutathione is part of a multicomponent system essential for mitochondrial function, Proc. Natl. Acad. Sci. USA 87 (18) (1990) 7185–7189.
[14] R.H. Houtkooper, C. Argmann, S.M. Houten, C. Canto, E.H. Jeninga, P. A. Andreux, C. Thomas, R. Doenlen, K. Schoonjans, J. Auwerx, The metabolic footprint of aging in mice, Sci. Rep. 1 (2011) 134.
[15] L.A. Sena, N.S. Chandel, Physiological roles of mitochondrial reactive oxygen species, Mol. Cell 48 (2) (2012) 158–167.
[16] S.H. Jo, M.K. Son, H.J. Koh, S.M. Lee, I.H. Song, Y.O. Kim, Y.S. Lee, K.S. Jeong, W. B. Kim, J.W. Park, B.J. Song, T.L. Huh, Control of mitochondrial redox balance and cellular defense against oxidative damage by mitochondrial NADP+-dependent isocitrate dehydrogenase, J. Biol. Chem. 276 (19) (2001) 16168–16176.
[17] D.E. Koshland Jr., K. Walsh, D.C. LaPorte, Sensitivity of metabolic fluxes to covalent control, Curr. Top. Cell. Regul. 27 (1985) 13–22.
[18] A. De Pauw, S. Tejerina, M. Raes, J. Keijer, T. Arnould, Mitochondrial (dys) function in adipocyte (de)differentiation and systemic metabolic alterations, Am. J. Pathol. 175 (3) (2009) 927–939.
[19] S. Kim, S.Y. Kim, H.J. Ku, Y.H. Jeon, H.W. Lee, J. Lee, T.K. Kwon, K.M. Park, J. W. Park, Suppression of tumorigenesis in mitochondrial NADP(+)-dependent isocitrate dehydrogenase knock-out mice, Biochim. Biophys. Acta 1842 (2) (2014) 135–143.
[20] Z.Y. Jiang, J.V. Hunt, S.P. Wolff, Ferrous ion oxidation in the presence of xylenol orange for detection of lipid hydroperoxide in low density lipoprotein, Anal. Biochem. 202 (2) (1992) 384–389.
[21] T.P. Akerboom, H. Sies, Assay of glutathione, glutathione disulfide, and glutathione mixed disulfides in biological samples, Methods Enzymol. 77 (1981) 373–382.
[22] M.E. Anderson, Determination of glutathione and glutathione disulfide in biological samples, Methods Enzymol. 113 (1985) 548–555.
[23] C.R. Zerez, S.J. Lee, K.R. Tanaka, Spectrophotometric determination of oxidized and reduced pyridine nucleotides in erythrocytes using a single extraction procedure, Anal. Biochem. 164 (2) (1987) 367–373.
[24] R.G. Spragg, D.B. Hinshaw, P.A. Hyslop, I.U. Schraufstatter, C.G. Cochrane, Alterations in adenosine triphosphate and energy charge in cultured endothelial and P388D1 cells after oxidant injury, J. Clin. Investig. 76 (4) (1985) 1471–1476.
[25] H.N. Ginsberg, Is the slippery slope from steatosis to steatohepatitis paved with triglyceride or cholesterol? Cell Metab. 4 (3) (2006) 179–181.
[26] Y. Matsuzawa, T. Funahashi, T. Nakamura, Molecular mechanism of metabolic syndrome X: contribution of adipocytokines adipocyte-derived bioactive substances, Ann. N. Y. Acad. Sci. 892 (1999) 146–154.
[27] K.T. Uysal, S.M. Wiesbrock, M.W. Marino, G.S. Hotamisligil, Protection from obesity-induced insulin resistance in mice lacking TNF-alpha function, Nature 389 (6651) (1997) 610–614.
[28] T. Yamauchi, J. Kamon, H. Waki, Y. Terauchi, N. Kubota, K. Hara, Y. Mori, T. Ide, K. Murakami, N. Tsuboyama-Kasaoka, O. Ezaki, Y. Akanuma, O. Gavrilova, C. Vinson, M.L. Reitman, H. Kagechika, K. Shudo, M. Yoda, Y. Nakano, K. Tobe, R. Nagai, S. Kimura, M. Tomita, P. Froguel, T. Kadowaki, The fat-derived hormone adiponectin reverses insulin resistance associated with both lipoatrophy and obesity, Nat. Med. 7 (8) (2001) 941–946.
[29] I. Shimomura, R.E. Hammer, S. Ikemoto, M.S. Brown, J.L. Goldstein, Leptin reverses insulin resistance and diabetes mellitus in mice with congenital lipodystrophy, Nature 401 (6748) (1999) 73–76.
[30] J.A. Levine, N.L. Eberhardt, M.D. Jensen, Role of nonexercise activity thermogenesis in resistance to fat gain in humans, Science 283 (5399) (1999) 212–214.
[31] J.D. Horton, Y. Bashmakov, I. Shimomura, H. Shimano, Regulation of sterol regulatory element binding proteins in livers of fasted and refed mice, Proc. Natl. Acad. Sci. USA 95 (11) (1998) 5987–5992.
[32] N. Yahagi, H. Shimano, T. Matsuzaka, Y. Najima, M. Sekiya, Y. Nakagawa, T. Ide, S. Tomita, H. Okazaki, Y. Tamura, Y. Iizuka, K. Ohashi, T. Gotoda, R. Nagai, S. Kimura, S. Ishibashi, J. Osuga, N. Yamada, p53 Activation in adipocytes of obese mice, J. Biol. Chem. 278 (28) (2003) 25395–25400.
[33] M. Harms, P. Seale, Brown and beige fat: development, function and therapeutic potential, Nat. Med. 19 (10) (2013) 1252–1263.
[34] J. Robidoux, W. Cao, H. Quan, K.W. Daniel, F. Moukdar, X. Bai, L.M. Floering, S. Collins, Selective activation of mitogen-activated protein (MAP) kinase kinase 3 and p38alpha MAP kinase is essential for cyclic AMP-dependent UCP1 expression in adipocytes, Mol. Cell. Biol. 25 (13) (2005) 5466–5479.
[35] R.C. Scarpulla, Metabolic control of mitochondrial biogenesis through the PGC-1 family regulatory network, Biochim. Biophys. Acta 1813 (7) (2011) 1269–1278.
[36] S. Kajimura, M. Saito, A new era in brown adipose tissue biology: molecular control of brown fat development and energy homeostasis, Annu. Rev. Physiol. 76 (2014) 225–249.
[37] M.T. Ryan, N.J. Hoogenraad, Mitochondrial-nuclear communications, Annu. Rev. Biochem. 76 (2007) 701–722.
[38] J.A. McCubrey, M.M. Lahair, R.A. Franklin, Reactive oxygen species-induced activation of the MAP kinase signaling pathways, Antioxid. Redox Signal. 8 (9–10) (2006) 1775–1789.

[39] B. Liu, Y. Chen, D.K. St Clair, ROS and p53: a versatile partnership, Free Radic. Biol. Med. 44 (8) (2008) 1529–1535.
[40] K. Apel, H. Hirt, Reactive oxygen species: metabolism, oxidative stress, and signal transduction, Annu. Rev. Plant Biol. 55 (2004) 373–399.
[41] W. Cao, K.W. Daniel, J. Robidoux, P. Puigserver, A.V. Medvedev, X. Bai, L. M. Floering, B.M. Spiegelman, S. Collins, p38 mitogen-activated protein kinase is the central regulator of cyclic AMP-dependent transcription of the brown fat uncoupling protein 1 gene, Mol. Cell. Biol. 24 (7) (2004) 3057–3067.
[42] S.H. Ro, M. Nam, I. Jang, H.W. Park, H. Park, I.A. Semple, M. Kim, J.S. Kim, H. Park, P. Einat, G. Damari, M. Golikov, E. Feinstein, J.H. Lee, Sestrin2 inhibits uncoupling protein 1 expression through suppressing reactive oxygen species, Proc. Natl. Acad. Sci. USA 111 (21) (2014) 7849–7854.
[43] A. Maillet, S. Pervaiz, Redox regulation of p53, redox effectors regulated by p53: a subtle balance, Antioxid. Redox Signal. 16 (11) (2012) 1285–1294.
[44] C.R. Berkers, O.D. Maddocks, E.C. Cheung, I. Mor, K.H. Vousden, Metabolic regulation by p53 family members, Cell Metab. 18 (5) (2013) 617–633.
[45] X. Wang, X. Zhao, X. Gao, Y. Mei, M. Wu, A new role of p53 in regulating lipid metabolism, J. Mol. Cell Biol. 5 (2) (2013) 147–150.
[46] T. Finkel, Signal transduction by reactive oxygen species, J. Cell Biol. 194 (1) (2011) 7–15.
[47] R.B. Hamanaka, N.S. Chandel, Mitochondrial reactive oxygen species regulate cellular signaling and dictate biological outcomes, Trends Biochem. Sci. 35 (9) (2010) 505–513.
[48] D. Pitocco, M. Tesauro, R. Alessandro, G. Ghirlanda, C. Cardillo, Oxidative stress in diabetes: implications for vascular and other complications, Int. J. Mol. Sci. 14 (11) (2013) 21525–21550.
[49] G. Bjelakovic, D. Nikolova, C. Gluud, Antioxidant supplements and mortality, Curr. Opin. Clin. Nutr. Metab. Care 17 (1) (2014) 40–44.
[50] G. Bjelakovic, D. Nikolova, L.L. Gluud, R.G. Simonetti, C. Gluud, Antioxidant supplements for prevention of mortality in healthy participants and patients with various diseases, Cochrane Database Syst. Rev. 2 (2008) CD007176.
[51] M. Ristow, K. Zarse, A. Oberbach, N. Kloting, M. Birringer, M. Kiehntopf, M. Stumvoll, C.R. Kahn, M. Bluher, Antioxidants prevent health-promoting effects of physical exercise in humans, Proc. Natl. Acad. Sci. USA 106 (21) (2009) 8665–8670.